PAPER

Sigma-Delta Beamformer DOA Estimation for Distributed Array Radar

Toshihiro ITO[†,††a)], **Shoji MATSUDA**[†††], ***and*** **Yoshiya KASAHARA**[††††], ***Members***

SUMMARY Distributed array radars consist of multiple sub-arrays separated by tens to hundreds of wavelengths and can match narrow beamwidths with large-aperture, high-gain antennas. The physical independence of the sub-arrays contributes to significant structure flexibility and is one of the advantages of such radars. However, a typical problem is the grating lobes in the digital beam forming (DBF) beam pattern. Unfortunately, the need to suppress the generation of grating lobes makes the design of acceptable sub-array arrangements very difficult. A sigma-delta beam former direction of arrival (DOA) estimation method is proposed in this study to solve this problem. The proposed method performs DOA estimation by acquiring the difference signals in addition to the sum signals of all sub-arrays. The difference signal is typically used for monopulse DOA estimation in the phased array radar. The sigma-delta beamformer simultaneously has both advantages of DOA estimations using a distributed array with a large aperture length and using a sub-array that is not affected by the grating lobe. The proposed method can improve the DOA estimation accuracy over the conventional method under grating lobe situations and help the distributed array radar achieve flexibility in the sub-array arrangement. Numerical simulations are presented to verify the effectiveness of the proposed DOA estimation method.

key words: *radar, distributed array, DOA estimation, beamformer, monopulse*

1. Introduction

Recently, distributed array radar (DAR) systems have received substantial interest and have been evaluated [1], [2]. DAR has a distributed array (DA) consisting of multiple sub-arrays (SA), which are phased array antennas; the coherent integration of the received signals of each SA is performed by digital beam forming (DBF). The DAR can realize the equivalent of a large-aperture, high-gain antenna radar system.

DAR systems have various advantages over conventional radar systems, such as, high detection performance owing to the integration of the SA signals, the flexibility of performance from the flexibility in the number of SAs, the flexibility of SA arrangement from the independence of the SA structure and ease of relocation from the SA transportability.

DAR has various advantages, as described above, but it also has many technical issues. For example, the large aperture length of the DA makes the transmitted beamwidth very narrow. In the case of surveillance radar [3], [4], the DAR must sequentially change the transmit beam in many directions, leading to a degradation of the search efficiency. This problem is resolved by using Multiple Input Multiple Output (MIMO) radar technology so that the transmitted signals from multiple transmitting SAs are not virtually combined prior to the DBF [5], [6]. However, selecting an orthogonal signal (modulation) is also an essential technical issue in MIMO radar [7].

Another typical problem is that the grating lobes (GL) occur in the DBF beam pattern owing to the larger distance between adjacent SAs. The GL are the lobes with higher response that occur at different angles from the desired beamforming direction. To suppress the generation of the GL, a non-uniform SA arrangement was evaluated [8], [9]. However, this SA arrangement to suppress the grating lobes has the disadvantage of reducing the flexibility of such an arrangement. Therefore, the DAR must operate even in a situation where the suppression of the grating lobes is insufficient to take advantage of the flexibility of the SA arrangement.

Typical of the radar signal processes affected by the grating lobes is the direction of the arrival (DOA) estimation process. The DOA estimation method for the DAR must operate with an arbitrary SA arrangement. A typical method with such a property is the beamformer DOA estimation [10]. Principally, the beamformer in digital signal processing is equivalent to the process of searching for a high gain angle while scanning the DBF beam direction in detail. Therefore, the GL angle may be incorrectly estimated as the target direction if a GL is in the DBF beam pattern.

This study proposes a new DOA estimation referred to as the Sigma-Delta beamformer ($\Sigma\Delta$BF) to solve this problem. One of the advantages of DAR is the flexibility of performance. This concept allows a single SA to operate as a radar in the case of the smallest configuration. Therefore, it is practical to assume that the SA has a DOA estimation function using SA aperture, and phase comparison monopulse is an established method for this method. The proposed method focuses on this point and performs DOA estimation by acquiring the difference signals used in each SA monopulse from all SAs in addition to the sum signals

Manuscript received December 22, 2021.
Manuscript revised April 8, 2022.
Manuscript publicized June 9, 2022.

[†]The author is with Information Technology R&D Center, Mitsubishi Electric Corp., Kamakura-shi, 247-8501 Japan.
[††]The author is with the Graduated School of Natural Science and Technology, Kanazawa University, Kanazawa-shi, 920-1192 Japan.
[†††]The author is with Communication Systems Center, Mitsubishi Electric Corp., Amagasaki-shi, 661-8661 Japan.
[††††]The author is with Emerging Media Initiative, Kanazawa University, Kanazawa-shi, 920-1192 Japan.
a) E-mail: Ito.Toshihiro@dy.MitsubishiElectric.co.jp
DOI: 10.1587/transcom.2021EBP3211

used in the conventional beamformer. The effect of this configuration is that the proposed method simultaneously obtains both advantages of the DOA estimations using DA with a large aperture length and using SA which is not affected by GL.

The remainder of this paper is organized as follows: In 2., the DAR assumed in this study and its typical functional structure is briefly presented. Additionally, the calculation results of GL in the case of a simple 1D distributed array are shown and the GL problem of DOA estimation is described. In 3., the concept of the ΣΔBF is described, and a typical signal processing flow of the proposed method is shown to clarify the integration of ΣΔBF into the DAR. Subsequently, the formulation of ΣΔBF DOA estimation is presented. In 4., the results of the computer simulations are presented to show that ΣΔBF has better DOA estimation accuracy than the conventional beamformer in the GL situation and that the accuracy of ΣΔBF depends on the SNR, DA structure, and SA structure. The concluding remarks of this study are presented in 5.

2. Problem Formulation

2.1 Distributed Array Radar

This study considers the DAR for a long-range target using DA consisting of multiple SAs arranged in the range of tens to hundreds of wavelengths. DA assumes far-field as conventional phased arrays. It is also assumed that the DAR is a pulse radar. Figure 1 shows an overview of the DAR and the typical functional structure after receiving. As shown in the left figure of Fig. 1, DA consists of multiple SAs. Each of these SAs is a planar phased array. The transmitting (or transmitting and receiving) SA directs a transmit pencil beam to the target, as in a conventional radar, and the receiving SA receives the reflected wave. As shown in Fig. 1, each receiving SA forms a beam (SA beam) by the analog phase control of the received signal. Based on the far-field assumption, the SA beams formed by each SA are synchronized and controlled in the same direction. The received signals of each SA beam are processed by analog signal processing, such as amplification, frequency conversion, and analog to digital (A/D). Subsequently, general pulse-Doppler radar digital signal processing, such as pulse compression and pulse Doppler processing (e.g., signal integration between pulse hits), is applied. The DBF process was performed to form DBF beams using SA received signals. Because DBF is digital processing, DBF beams are formed simultaneously in multiple directions to fill the beamwidth of the SA beam (multi-beam forming). Subsequently, the target detection and position estimation of the detected target is performed. DOA estimation is one of the critical functions of target position estimation, and it estimates the direction of the target within the SA beam.

The DAR has the following advantages:

- High Detection Performance
  Increasing the number of the SAs increases the transmit power and gain of the DA. Therefore, the detection performance is improved according to the radar equation [11].
- Flexibility of the Performance
  Performance can be adjusted by setting the number of SAs according to the required performance. Moreover, it is possible to respond to changes in the required performance by changing the number of SAs. A single SA can operate as a radar in the smallest configuration.
- Flexibility of SA Arrangement
  Because each SA is an independent structure, the SAs can be arranged flexibly according to the terrain and other requirements.
- Ease of Relocation
  If the size and weight of the SA are designed such that it can be transported, the DAR can be relocated by vehicle or other transportation methods.

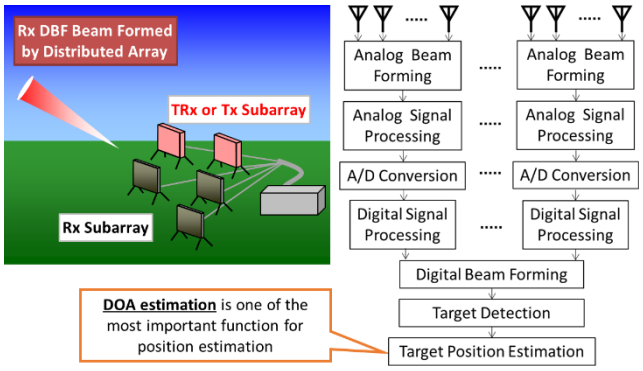

Fig. 1 Overview of distributed array radar and typical functional structure after receiving.

2.2 DOA Estimation Error due to Grating Lobe

The DBF beam pattern against the angle depends on the SA arrangement. When the distances between each SA are wide, GLs are generated at angles different from the desired beam direction in the DBF beam pattern. Figure 2 shows a typical example of a DBF beam pattern in the presence of GL. This example simulates a DA with five SAs arranged uniformly in one dimension. The number of elements per SA was 28, and the distance between the elements was half a wavelength. The distance between the phase centers of the adjacent SAs was 30 wavelengths. The desired DBF beam forming direction is set to 0° in Fig. 2. The angles of the GLs in the case of a uniformly arranged array when the DBF beam direction is 0° are generally expressed by

$$\theta_{GL} = \sin^{-1} \frac{n\lambda}{d_c} \tag{1}$$

where n, λ, and d_c represent a non-zero integer, wavelength, and distance between the phase centers of adjacent SAs, respectively. In the case of Fig. 2, θ_{GL} calculated from Eq. (1) is 1.91° ($n = 1$) and −1.91° ($n = -1$), and GLs occur at

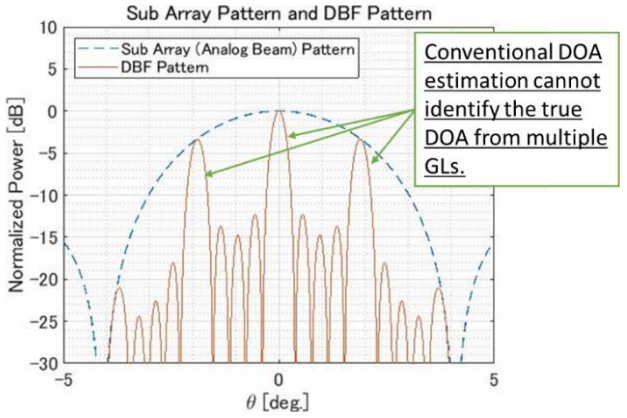

Fig. 2 Typical example of sub array pattern and DBF pattern with GL. The desired DBF beam forming direction is 0°, and θ_{GL} is −1.91° ($n = -1$) and 1.91° ($n = 1$).

the directions shown in the figure. It is important to note that the GL occurs within the SA beam in Fig. 2. A conventional DOA estimation process applied to any antenna arrangement, such as a non-uniform arrangement, is a beamformer [10] or methods derived from it. The beamformer in the digital signal processing is, in principle, a process of searching for an angle of high gain while scanning the DBF beam direction within the SA beam in detail. Hence, there is a risk of incorrectly estimating the angle of the GL as the target direction when the GL exists, as shown in Fig. 2.

Previous studies have shown that a non-uniform SA arrangement effectively suppresses the generation of GL [8], [9]. In this approach, the non-uniform SA arrangement prevents the SA signals from being combined in-phase, except at the desired beamforming direction. However, to sufficiently suppress the GL, it is necessary to impose strict constraints on the SA arrangement. As mentioned before, one of the advantages of DAR is the flexibility of the SA arrangement. The constraints on the SA arrangement may undermine this advantage. Therefore, it is useful to have a method that minimizes the accuracy loss of the DOA estimation even when the GL is not sufficiently suppressed. ΣΔBF is proposed as a method in the next section.

3. Proposed Sigma-Delta Beamformer DOA Estimation

3.1 Concept of the Proposed Sigma-Delta Beamformer

The beamformer described in 2.2 can be considered a DOA estimation using the DA aperture. However, it is assumed that the DOA estimation using the SA aperture is given in DAR. This is because the minimum configuration of the DAR is a single SA radar operation, as described in 2.1. A phase comparison monopulse is an established single-target DOA estimation technique in phased array radar, such as a single SA situation [12], [13]. This method has a good accuracy and requires a low amount of calculation. To estimate both the elevation and azimuth angles, monopulse is realized by dividing the antenna plane into four identical gain regions, making one sum signal and two difference signals, and utilizing the relationship between the DOA and the three signals. The sum signal is generated by summing the signals of the four regions. In other words, it is equal to the ordinary output signal from the SA. One of the difference signals is generated by the vertical difference of the signals in the four regions, and the horizontal difference generates the other.

Table 1 Comparison of beamformer DOA estimation using DA with GL and monopulse DOA estimation using SA.

	Beamformer using DA with GL	Monopulse using SA
Theoretical limit of DOA accuracy	**good**	poor
	Because DA aperture is larger than SA aperture.	
Uniqueness of the estimation within SA beam	not unique	**unique**
	Because monopulse does not use DA aperture.	

Table 1 compares the conventional beamformer using DA and monopulse using only SA. The accuracy limit of the DOA estimation in ideal behavior is generally better when the aperture length is larger; thus, the theoretical limit of the accuracy of the beamformer using a larger DA aperture is better than that of a monopulse. In contrast, the beamformer has the GL problem, but the monopulse does not because it does not use a DA aperture. It can be observed that the advantages and disadvantages of the two methods complement each other.

The concept of the proposed ΣΔBF is simple; it involves performing the DOA estimation process using all the input signals used by these two methods simultaneously. This method aims to provide a DOA estimation that simultaneously combines the complementary properties of the two methods.

Figure 3 shows a typical signal processing flow of DAR including ΣΔBF. We assume that each SA outputs the sum signal and two difference signals. Parameters Σ_m, $\Delta_{u,m}$ and $\Delta_{v,m}$ denote the three signals of the mth SA after the A/D conversion, pulse compression, and pulse Doppler processing, respectively. A target detection process, such as CFAR [11] after DBF, detects the target signal when the target is present. The target detection process provides the $x_{\Sigma\Delta}$ extraction process with information on the target range cell number $\hat{n}_R$ and target Doppler cell number $\hat{n}_D$, where hat denotes the estimation. The $\boldsymbol{x}_{\Sigma\Delta}$ extraction process extracts the complex amplitudes of the cells specified by $\hat{n}_R$ and $\hat{n}_D$ in Σ_m, $\Delta_{u,m}$ and $\Delta_{v,m}$ of all the SAs and generates the complex vector $\boldsymbol{x}_{\Sigma\Delta}$. The $\boldsymbol{x}_{\Sigma\Delta}$ is added to the ΣΔBF process. It should be noted that, as in the case with the conventional monopulse, we assume that there is only one target for which the detected target range, target Doppler, and SA beam are all identical. This means that $\boldsymbol{x}_{\Sigma\Delta}$ is a complex amplitude vector corresponding to a single target. The ΣΔBF process performs DOA estimation and outputs the elevation angle estimation $\hat{\theta}_{\Sigma\Delta}$ and azimuth angle estimation

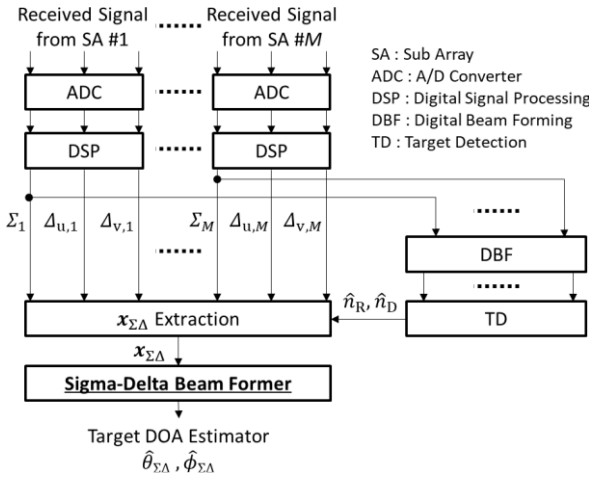

Fig. 3 Typical signal processing flow of a distributed array radar including proposed ΣΔBF.

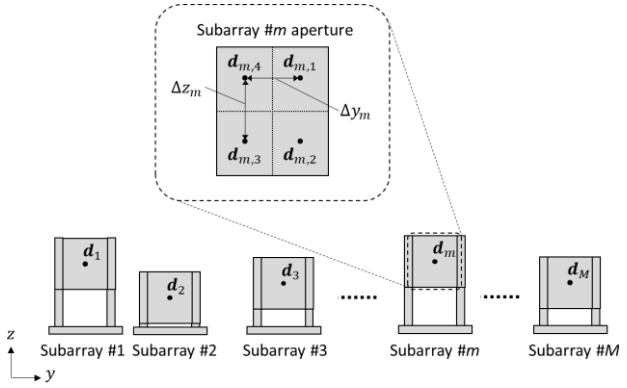

Fig. 4 Model of distributed array used for proposed ΣΔBF.

$\hat{\phi}_{\Sigma\Delta}$. The details of the ΣΔBF are formulated in the next section.

3.2 Formulation of the Sigma-Delta Beamformer

The signal model is organized in this section, and the ΣΔBF is formulated. As described above, we assume far-field and single-target DOA estimation. Additionally, we do not consider the multipath environment.

Figure 4 shows the DA model used for the proposed ΣΔBF. Parameter $\boldsymbol{d}_m$ in this figure denotes the phase center position vector of the mth SA, as shown below:

$$\boldsymbol{d}_m = \begin{bmatrix} x_m & y_m & z_m \end{bmatrix}^{\mathrm{T}} \tag{2}$$

where m and T represent the SA index number and transpose, respectively. Parameter $\boldsymbol{d}_{m,n}$ in Fig. 4, and n denote the phase center position vectors of the four regions in the mth SA and region number. The relationship between $\boldsymbol{d}_m$ and $\boldsymbol{d}_{m,n}$ can be written as

$$\boldsymbol{d}_{m,n} = \boldsymbol{d}_m + \Delta\boldsymbol{d}_{m,n} \tag{3}$$

where $\Delta\boldsymbol{d}_{m,n}$ is given by

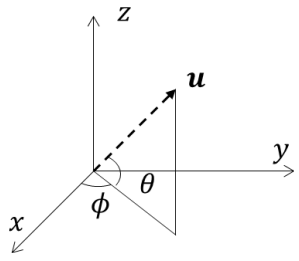

Fig. 5 Coordinate system in this paper.

$$\Delta\boldsymbol{d}_{m,1} = \begin{bmatrix} 0 & \Delta y_m/2 & \Delta z_m/2 \end{bmatrix}^{\mathrm{T}} \tag{4}$$

$$\Delta\boldsymbol{d}_{m,2} = \begin{bmatrix} 0 & \Delta y_m/2 & -\Delta z_m/2 \end{bmatrix}^{\mathrm{T}} \tag{5}$$

$$\Delta\boldsymbol{d}_{m,3} = \begin{bmatrix} 0 & -\Delta y_m/2 & -\Delta z_m/2 \end{bmatrix}^{\mathrm{T}} \tag{6}$$

$$\Delta\boldsymbol{d}_{m,4} = \begin{bmatrix} 0 & -\Delta y_m/2 & \Delta z_m/2 \end{bmatrix}^{\mathrm{T}} \tag{7}$$

where Δy_m and Δz_m represent the lengths between the phase centers of the two regions in the horizontal and vertical directions, respectively, and these lengths are referred to as monopulse lengths in this study.

Using this DA model, the complex amplitude of the target signal at the nth region of the mth SA can be expressed as

$$\begin{aligned} x_{m,n} = \exp\left\{ j\frac{2\pi}{\lambda}\left(\boldsymbol{d}_{m,n}^T\boldsymbol{u} - \Delta\boldsymbol{d}_{m,n}^T\boldsymbol{u_0}\right)\right\} \\ \cdot G_m\left(u-u_0, v-v_0\right) s \end{aligned} \tag{8}$$

where $G_m(-)$ and s denote the gain pattern of each region of the mth SA and the complex amplitude of the target reflection signal, respectively. Parameters $\boldsymbol{u}$ and $\boldsymbol{u_0}$ are the DOA vector and SA beam direction vector, respectively. This study used the coordinate system shown in Fig. 5. In this case, the relationship between $\boldsymbol{u}$, u, v and elevation angle θ, and azimuth angle ϕ is as follows:

$$\begin{aligned} \boldsymbol{u} &= \begin{bmatrix} \sqrt{1-u^2-v^2} & u & v \end{bmatrix}^{\mathrm{T}} \\ &= \begin{bmatrix} \cos\theta\cos\phi & \cos\theta\sin\phi & \sin\theta \end{bmatrix}^{\mathrm{T}}. \end{aligned} \tag{9}$$

The relationship between $\boldsymbol{u}_0$ and the SA beam elevation angle θ_0, azimuth angle ϕ_0 is the same as in Eq. (9).

The target reflection signal of the mth sum signal $x_{\Sigma,m}$, the mth difference signals $x_{u,m}$ and $x_{v,m}$ can be described as

$$x_{\Sigma,m} = x_{m,1} + x_{m,2} + x_{m,3} + x_{m,4} \tag{10}$$

$$x_{u,m} = x_{m,1} + x_{m,2} - x_{m,3} - x_{m,4} \tag{11}$$

$$x_{v,m} = x_{m,1} - x_{m,2} - x_{m,3} + x_{m,4}. \tag{12}$$

Substituting Eq. (3), Eq. (4), Eq. (5), Eq. (6), Eq. (7) and Eq. (8), and using the relationship $\exp(j\alpha) + \exp(-j\alpha) = 2\cos\alpha$ and $\exp(j\alpha) - \exp(-j\alpha) = j2\sin\alpha$, Eq. (10), Eq. (11) and Eq. (12) are transformed as follows:

$$x_{\Sigma,m} = 4 \cdot G_m(u-u_0, v-v_0) \cdot \exp\left(j\frac{2\pi}{\lambda}\boldsymbol{d}_m^T\boldsymbol{u}\right) \cdot \cos\left\{\frac{\pi}{\lambda}\Delta y_m(u-u_0)\right\}\cos\left\{\frac{\pi}{\lambda}\Delta z_m(v-v_0)\right\}\cdot s \tag{13}$$

$$x_{u,m} = j4 \cdot G_m(u-u_0, v-v_0) \cdot \exp\left(j\frac{2\pi}{\lambda}\boldsymbol{d}_m^T\boldsymbol{u}\right) \cdot \sin\left\{\frac{\pi}{\lambda}\Delta y_m(u-u_0)\right\}\cos\left\{\frac{\pi}{\lambda}\Delta z_m(v-v_0)\right\}\cdot s \tag{14}$$

$$x_{v,m} = j4 \cdot G_m(u-u_0, v-v_0) \cdot \exp\left(j\frac{2\pi}{\lambda}\boldsymbol{d}_m^T\boldsymbol{u}\right) \cdot \cos\left\{\frac{\pi}{\lambda}\Delta y_m(u-u_0)\right\}\sin\left\{\frac{\pi}{\lambda}\Delta z_m(v-v_0)\right\}\cdot s. \tag{15}$$

Extracting only the terms that depend on u and v in Eq. (13), Eq. (14), and Eq. (15), the element factors $a_{\Sigma,m}$, $a_{u,m}$, and $a_{v,m}$ for ΣΔBF are as follows:

$$a_{\Sigma,m} = G_m(u-u_0, v-v_0) \cdot \exp\left(j\frac{2\pi}{\lambda}\boldsymbol{d}_m^T\boldsymbol{u}\right) \cdot \cos\left\{\frac{\pi}{\lambda}\Delta y_m(u-u_0)\right\}\cos\left\{\frac{\pi}{\lambda}\Delta z_m(v-v_0)\right\} \tag{16}$$

$$a_{u,m} = j \cdot G_m(u-u_0, v-v_0) \cdot \exp\left(j\frac{2\pi}{\lambda}\boldsymbol{d}_m^T\boldsymbol{u}\right) \cdot \sin\left\{\frac{\pi}{\lambda}\Delta y_m(u-u_0)\right\}\cos\left\{\frac{\pi}{\lambda}\Delta z_m(v-v_0)\right\} \tag{17}$$

$$a_{v,m} = j \cdot G_m(u-u_0, v-v_0) \cdot \exp\left(j\frac{2\pi}{\lambda}\boldsymbol{d}_m^T\boldsymbol{u}\right) \cdot \cos\left\{\frac{\pi}{\lambda}\Delta y_m(u-u_0)\right\}\sin\left\{\frac{\pi}{\lambda}\Delta z_m(v-v_0)\right\}. \tag{18}$$

Using the signal model presented above, ΣΔBF is realized as the maximum value search in the following equation:

$$\left\{\hat{\theta}_{\Sigma\Delta}, \hat{\phi}_{\Sigma\Delta}\right\} = \arg\max \frac{\boldsymbol{a}_{\Sigma\Delta}^{\mathrm{H}}\boldsymbol{x}_{\Sigma\Delta}\boldsymbol{x}_{\Sigma\Delta}^{\mathrm{H}}\boldsymbol{a}_{\Sigma\Delta}}{\boldsymbol{a}_{\Sigma\Delta}^{\mathrm{H}}\boldsymbol{a}_{\Sigma\Delta}} \tag{19}$$

where $\boldsymbol{x}_{\Sigma\Delta}$ and H are the complex amplitude vectors of the observed target provided by the $x_{\Sigma\Delta}$ extraction process and the complex conjugate transpose, respectively. The structure of $\boldsymbol{x}_{\Sigma\Delta}$ is given by

$$\boldsymbol{x}_{\Sigma\Delta} = \left[x_{\Sigma,1}, \cdots x_{\Sigma,M}, x_{u,1}, \cdots x_{u,M}, x_{v,1}, \cdots x_{v,M}\right]^{\mathrm{T}}. \tag{20}$$

Parameter $\boldsymbol{a}_{\Sigma\Delta}$ is the calculated steering vector for ΣΔBF, and its elements are the element factors $a_{\Sigma,m}$, $a_{u,m}$, and $a_{v,m}$ as shown below:

$$\boldsymbol{a}_{\Sigma\Delta} = \left[a_{\Sigma,1}, \cdots a_{\Sigma,M}, a_{u,1}, \cdots a_{u,M}, a_{v,1}, \cdots a_{v,M}\right]^{\mathrm{T}}. \tag{21}$$

In the case of the DAR in this study, an arbitrary range is set for θ and ϕ within the SA beam, and the calculated values of Eq. (16), Eq. (17), Eq. (18), and Eq. (21) for this range were used to solve Eq. (19).

It should be noted that when all SAs have the same structure, $G_m(u-u_0, v-v_0)$ can be omitted in the calculation of Eq. (16), Eq. (17) and Eq. (18). Because $G_m(u-u_0, v-v_0)$ is identical for all m and there is no information in the comparison of each element of $\boldsymbol{x}_{\Sigma\Delta}$.

To compare the conventional and proposed methods, we also formulate the conventional beamformer for a single target using the same signal model. As described in 2.2, the conventional beamformer is equivalent to the process of scanning the DBF beam to find a high gain angle, and the DBF beam is formed by integrating the sum signals of each SA. Therefore, the conventional beamformer is a maximum power search using only $\boldsymbol{x}_{\Sigma}$ and $\boldsymbol{a}_{\Sigma}$. The formulation of the conventional beamformer is as follows:

$$\boldsymbol{x}_{\Sigma} = \left[x_{\Sigma,1}, \cdots x_{\Sigma,M}\right]^{\mathrm{T}} \tag{22}$$

$$\boldsymbol{a}_{\Sigma} = \left[a_{\Sigma,1}, \cdots a_{\Sigma,M}\right]^{\mathrm{T}} \tag{23}$$

$$\left\{\hat{\theta}_{\Sigma}, \hat{\phi}_{\Sigma}\right\} = \arg\max \frac{\boldsymbol{a}_{\Sigma}^{\mathrm{H}}\boldsymbol{x}_{\Sigma}\boldsymbol{x}_{\Sigma}^{\mathrm{H}}\boldsymbol{a}_{\Sigma}}{\boldsymbol{a}_{\Sigma}^{\mathrm{H}}\boldsymbol{a}_{\Sigma}}. \tag{24}$$

The structure of the evaluation function of the ΣΔBF in Eq. (19) is the same as that of the conventional beamformer in Eq. (24). The only difference is whether the difference signals are used as input. In this paper, we refer to the conventional beamformer using Eq. (24) as ΣBF because of the difference between the two structures. Therefore, as intended, the addition of the difference signals makes ΣΔBF a method that behaves differently from conventional methods. Additionally, the ΣΔBF is equivalent to the maximum likelihood estimation (MLE) using the same signal model (see Appendix A).

4. Evaluation

In this section, the performance of the proposed ΣΔBF is evaluated by computer simulation, and its properties are discussed.

4.1 Evaluation of the Properties against Distributed Array Aperture Length

First, we evaluated the properties against the distributed array aperture length. Table 2 lists the simulation conditions, and Fig. 6 shows the SA arrangement used in this section and the subsequent sections. The target SNR in Table 2 indicates the ideal SNR after DBF when the target is at the center of the SA and DBF beams. The SA arrangement consists of the upper and lower regions, and each region is composed of 10 SAs with a random arrangement. The parameter ΔH stands for the height difference between the two regions, as shown in Fig. 6. In this arrangement, GL occurs at the elevation angle because of the large vertical gaps. Therefore, we evaluated the elevation angle estimation $\hat{\theta}_{\Sigma\Delta}$. The simulation evaluates the root mean squared error (RMSE) of the proposed ΣΔBF and the conventional ΣBF while varying ΔH.

Figure 7 shows the RMSE of the elevation angle estimation. In addition to the RMSE, the calculation results of

Table 2 Simulation conditions in 4.1.

Item	condition	note
Number of subarray	20	All subarrays have the same configuration
SA arrangement	Randomly arranged subarrays at two different heights	The upper and lower regions each consist of 10 SAs as shown in Fig. 6
Height difference ΔH	$5\lambda \sim 50\lambda$	ΔH is shown in Fig. 6
Monopulse length $\Delta y_m, \Delta z_m$	7λ	Same for all subarrays
SA beam direction	Elevation : 0° Azimuth : 0°	
Target SNR	20dB	
Target DOA	Elevation : 1° Azimuth : 0°	
Number of trials	2000	In each ΔH case

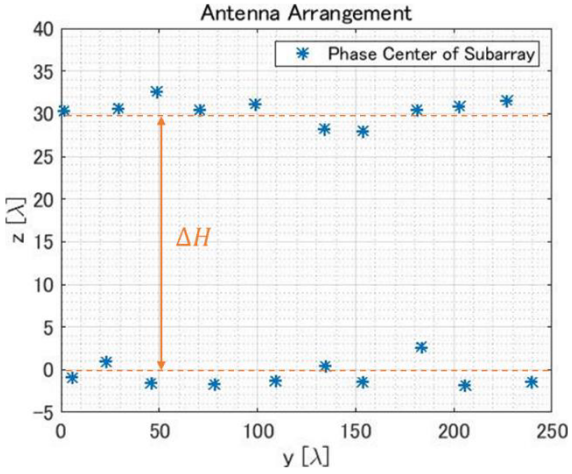

Fig. 6 Subarray arrangement used for simulation (in the case of a height difference of 30 wavelength).

the CRLB (Cramer-Rao Lower Bound) of ΣΔBF and ΣBF are also shown (see Appendix B). In the case of the Gaussian error distribution, MLE is asymptotic to the CRLB [14], and, as mentioned before, ΣΔBF is consistent with MLE using $\boldsymbol{x}_{\Sigma\Delta}$ and $\boldsymbol{a}_{\Sigma\Delta}$. If the estimation is not affected by GL, the error distribution of the DOA estimation should be Gaussian around the true DOA; therefore, the RMSE of the estimation should be asymptotic to the CRLB. Therefore, this evaluation uses the comparison between the RMSE and CRLB as an indicator of whether the estimation is affected by the GL. Figure 7 shows that the RMSE of the conventional ΣBF deviates from the CRLB as ΔH increases. This indicates that the GL degrades the accuracy of the ΣBF. However, the RMSE of ΣΔBF asymptotically approaches the CRLB, although there is a slight deviation when ΔH is approximately 50λ. To further analyze this result, Fig. 8 shows the number of outlier occurrences during 2000 trials. The formulas for

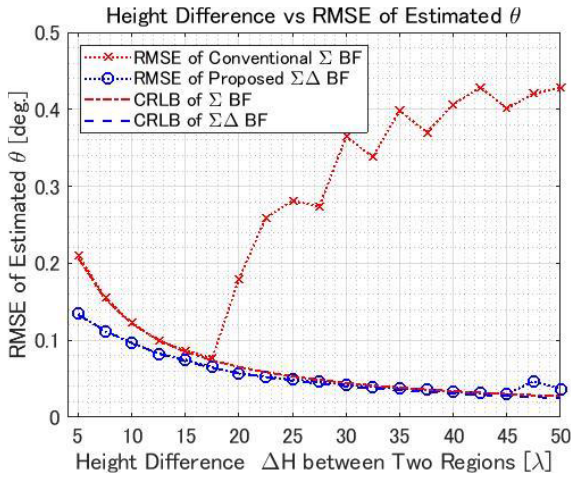

Fig. 7 RMSE of elevation angle estimation results and CRLB against height difference between two regions.

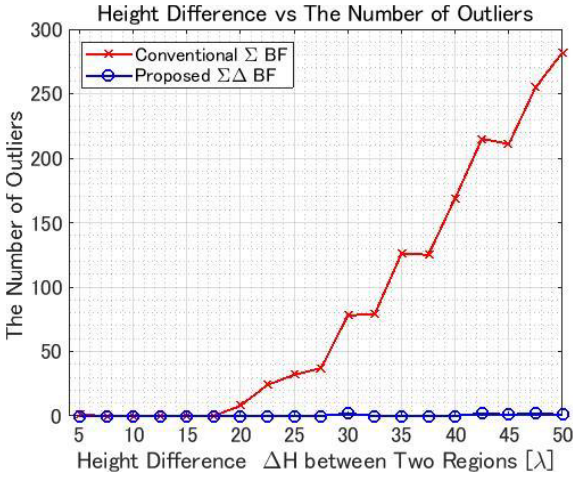

Fig. 8 Number of outlier occurrences against height difference between two regions.

determining the outliers of ΣΔBF and ΣBF used in Fig. 8 is shown below:

$$\frac{\left|\hat{\theta}_{\Sigma\Delta} - \theta_{\text{true}}\right|}{\sigma_{\Sigma\Delta,\theta}} > c_{\text{thre}} \tag{25}$$

$$\frac{\left|\hat{\theta}_{\Sigma} - \theta_{\text{true}}\right|}{\sigma_{\Sigma,\theta}} > c_{\text{thre}} \tag{26}$$

where θ_{true}, $\sigma_{\Sigma\Delta,\theta}$ and $\sigma_{\Sigma,\theta}$ represent the true elevation angle of the target, CRLB of ΣΔBF and ΣBF. c_{thre} denote the determination threshold. As described before, if there is no GL influence, the estimation becomes the Gaussian distribution centered on θ_{true} and its standard deviation asymptotically approaches the CRLB. In the evaluation shown in Fig. 8, the estimation that departs from the Gaussian distribution is determined as an outlier by setting $c_{\text{thre}} = 3$. In other words, Fig. 8 can be regarded as an evaluation of the number of estimations affected by GL. In the results of Fig. 8, the number of the ΣBF outliers increases rapidly with increasing ΔH when ΔH is greater than 20λ. From Eq. (1),

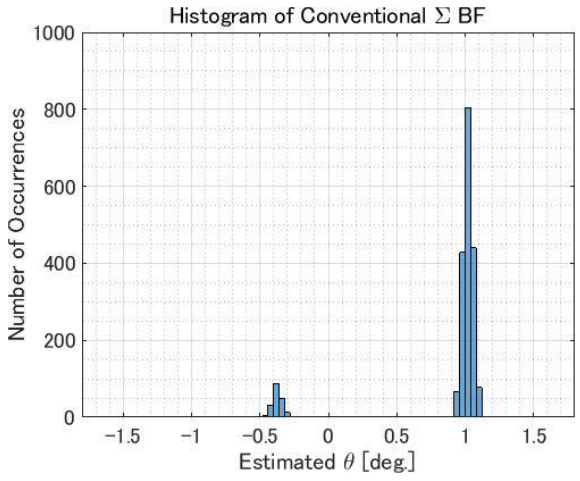

Fig. 9 Histogram of elevation angle estimation results by conventional ΣBF in case of SNR is 20 dB and height difference of 40 wavelength.

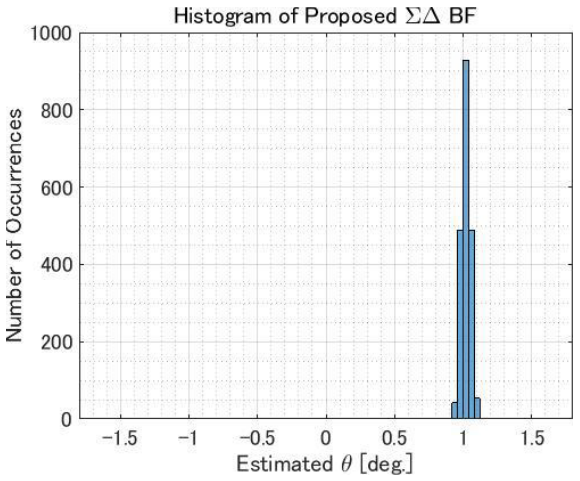

Fig. 10 Histogram of elevation angle estimation results by proposed ΣΔBF in case of SNR is 20 dB and height difference of 40 wavelength.

the θ_{GL} for $n = 1$ becomes smaller as ΔH increases. The subarray arrangement in Fig. 6 has the effect of slightly reducing GL by applying a random arrangement to each of the upper and lower regions. However, as θ_{GL} decreases, the reduction effect also decreases (see Appendix C). Therefore, as ΔH increases, the GL is affected more strongly, and the number of outliers increases. Additionally, from Eq. (1), the difference between θ_{GL} and θ_{true} decreases as ΔH increases. Therefore, the error in the case of incorrect estimation due to GL decreases as ΔH increases. However, the increase in the number of ΣBF outliers shown in Fig. 8 is more significant; consequently, the RMSE of ΣBF increases with increasing ΔH as shown in Fig. 7. In contrast, the outliers in ΣΔBF occur very seldom as shown in Fig. 8. This result suggests that the ΣΔBF estimations are concentrated around θ_{true} and that the effect of GL is well suppressed. Therefore, it can be observed that ΣΔBF can estimate the DOA while suppressing the influence of GL even when GL is not sufficiently suppressed.

To confirm the distribution of the estimations, histograms of the ΣBF estimations and the ΣΔBF estimations at $\Delta H = 40\lambda$ are shown in Fig. 9 and Fig. 10. In the results of Fig. 9, there is a distribution of estimations corresponding to the true DOA around 1°, but there is also a distribution of estimations at approximately −0.4°. We then consider the angle of GL in this evaluation. Substituting $d_c = \Delta H$ and $n = -1$ in Eq. (1) leads to $\theta_{GL} \approx -1.4°$. Because θ_{GL} in Eq. (1) is the angle of GL when $\theta_{\text{true}} = 0°$, when $\theta_{\text{true}} = 1°$, the angle of GL becomes $1° - 1.4° = -0.4°$. Therefore, the distribution at approximately −0.4° in Fig. 9 is due to the estimations corresponding to the GL. In contrast, only the distribution corresponding to the true DOA is shown in Fig. 10, and the number of occurrences of the true DOA distribution is improved compared to Fig. 9. The above results also confirmed the effect of the GL suppression.

Table 3 Simulation conditions in 4.2.

Item	condition	note
Number of subarray	20	All subarrays have the same configuration
SA arrangement	Randomly arranged subarrays at two different heights	The upper and lower regions each consist of 10 SAs as shown in Fig. 6
Height difference ΔH	30λ	ΔH is shown in Fig. 6
Monopulse length $\Delta y_m, \Delta z_m$	7λ	Same for all subarrays
SA beam direction	Elevation : 0° Azimuth : 0°	
Target SNR	15 ~ 25dB	
Target DOA	Elevation : 1° Azimuth : 0°	
Number of trials	2000	In each SNR case

4.2 Evaluation of the Properties against Target SNR

This section evaluates the properties of ΣΔBF against the target SNR. Table 3 lists the simulation conditions for this section. The SA arrangement is the same as in 4.1, as shown in Fig. 6; however, the height difference ΔH is fixed at 30λ. The target SNR varied from 15 dB to 25 dB.

Figure 11 shows the results of the evaluated RMSE and calculated CRLB against the target SNR. Figure 12 also shows the number of outlier occurrences against the target SNR. The results of ΣΔBF and ΣBF are shown in both figures. In Fig. 11, the RMSE of ΣΔBF deviates from the CRLB when the target SNR is relatively low. The proposed ΣΔBF can be interpreted as a method for estimating and solving the ambiguity of the DOA estimator by GL using the SA aperture monopulse. When the target SNR is low,

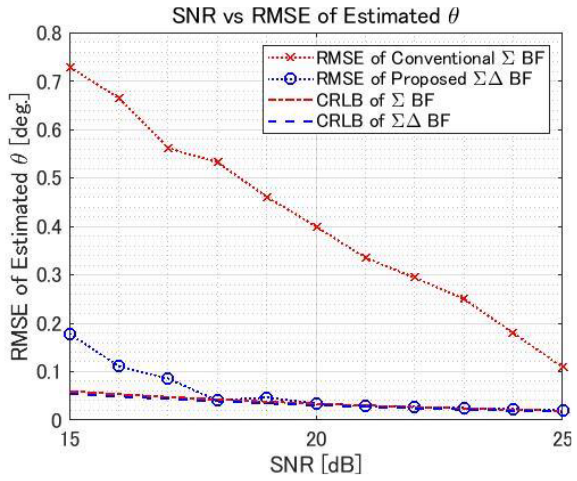

Fig. 11 RMSE of elevation angle estimation results and CRLB against target SNR.

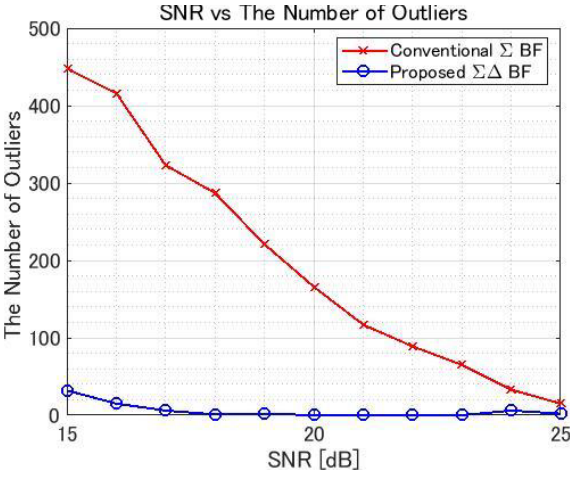

Fig. 12 Number of outlier occurrences against target SNR.

the accuracy of the SA aperture monopulse also decreases, and the solution to the ambiguity may be erroneous; therefore, the GL suppression performance is slightly degraded. The result of ΣΔBF in Fig. 12 also shows that even ΣΔBF generates some outliers when SNR is relatively low. However, the RMSE and the number of outlier occurrences for ΣΔBF were better than ΣBF in all the SNR cases. In other words, ΣΔBF has a lower SNR affected by GL than conventional DOA estimation using DA.

4.3 Evaluation of the Properties against Monopulse Length

As mentioned previously, ΣΔBF utilizes the SA aperture monopulse. Because the performance of the monopulse depends on the monopulse length, the performance of ΣΔBF is also supposed to depend on it. Thus, the properties of ΣΔBF against the monopulse length are evaluated in this section. The simulation conditions are listed in Table 4. In this simulation, the monopulse lengths Δy and Δz varied from 1λ to 10λ, and all other conditions were fixed values as presented in Table 4.

Table 4 Simulation conditions in 4.3.

Item	condition	note
Number of subarray	20	All subarrays have the same configuration
SA arrangement	Randomly arranged subarrays at two different heights	The upper and lower regions each consist of 10 SAs as shown in Fig. 6
Height difference ΔH	30λ	ΔH is shown in Fig. 6
Monopulse length $\Delta y_m, \Delta z_m$	$1\lambda \sim 10\lambda$	Same for all subarrays
SA beam direction	Elevation : 0° Azimuth : 0°	
Target SNR	20 dB	
Target DOA	Elevation : 1° Azimuth : 0°	
Number of trials	2000	In each SNR case

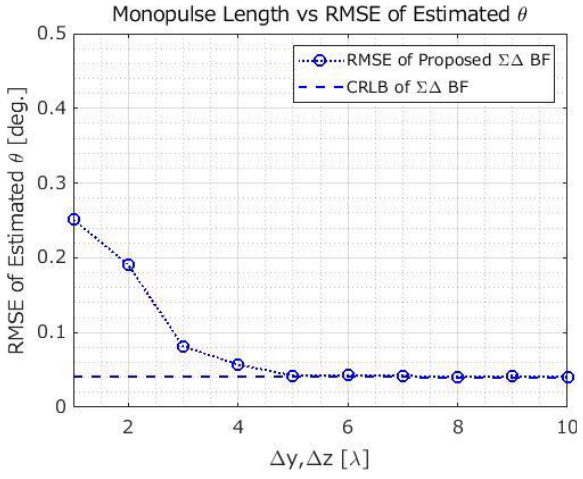

Fig. 13 RMSE of elevation angle estimation results and CRLB against monopulse length.

Figure 13 shows the RMSE and CRLB of ΣΔBF against the monopulse length Δy and Δz. Because ΣBF does not use $\boldsymbol{x}_u$ and $\boldsymbol{x}_v$, unlike previous evaluations, ΣBF was not evaluated in this section. Additionally, Fig. 14 shows the number of outlier occurrences of ΣΔBF against the monopulse length Δy and Δz. Figure 13 shows whether the RMSE of ΣΔBF reaching the CRLB depends on the monopulse length. Figure 14 also shows that the number of outliers increases as the monopulse length decreases. This is because of the accuracy of the monopulse, in other words, the effect of using $\boldsymbol{x}_u$ and $\boldsymbol{x}_v$, increases for larger monopulse lengths [12]. This evaluation result suggests that it is essential to design the SA with appropriate monopulse lengths Δy and Δz according to other assumed parameters, such as the maximum range of the SA arrangement and minimum target

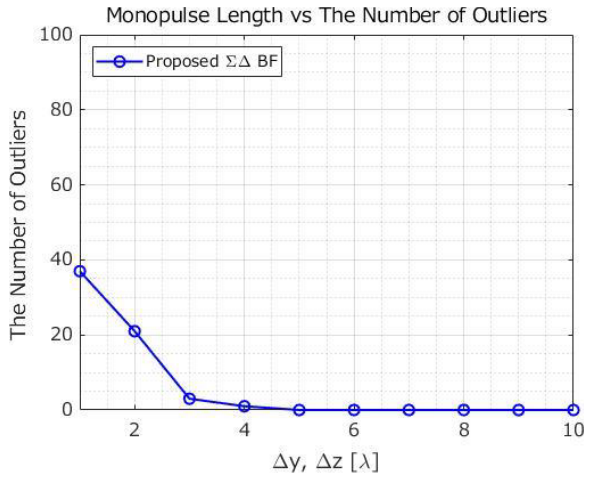

Fig. 14 Number of outlier occurrences against monopulse length.

SNR.

5. Conclusion

The ΣΔBF used to solve the problem of DOA accuracy degradation due to GL occurring in DAR was proposed in this study. The proposed method performs DOA estimation by acquiring the difference signals used in each SA monopulse from all SAs, in addition to the sum signals. The proposed method simultaneously obtains both advantages of the DOA estimations using DA with a large aperture length and SA which is not affected by GL.

The simulation results showed that the ΣΔBF has better DOA estimation accuracy than the conventional beamformer in the GL situation and that the accuracy of the ΣΔBF depends on the SNR, DA structure, and SA structure. These results suggest that it is important to design the SA to have appropriate monopulse lengths according to other assumed parameters, such as the maximum range of the SA arrangement and minimum target SNR. We demonstrated that the ΣΔBF can help the DAR to achieve the flexibility of the SA arrangement when the SA is appropriately designed. It should be noted that the proposed ΣΔBF is for a single target as described in 3. Although ΣΔBF does not have multiple-target separation capability, a radar equipped with ΣΔBF can separate multiple targets using range and Doppler resolution as well as conventional radars [11], [15].

However, the current ΣΔBF algorithm needs to calculate Eq. (16), Eq. (17) and Eq. (18) for all θ and ϕ within the SA beam. Therefore, the calculation amount increases when the SA beam width is large. The future work will be to solve the minimization problem of Eq. (19) more efficiently and reduce the amount of calculation.

References

[1] R.C. Heimiller, P.G. Tomlinson, and J.E. Belyea, "Distributed array radar," IEEE Trans. Aerosp. Electron. Syst., vol.AES-19, no.6, pp.831–839, 1983.
[2] W.L. Melvin, R. Hancock, M. Rangaswamy, and J. Parker, "Adaptive distributed radar," 2009 IEEE Radar Conference, pp.1–6, 2009.
[3] T. Roy, D. Meena, and L.G.M. Prakasam, "Comparison of efficient design techniques for surveillance radars," 2007 IEEE Radar Conference, June 2007.
[4] Y. Brihenche, F. Barbaresco, F. Bennis, and D. Chablat, "Optimisation of radar search patterns in localised clutter and terrain masking under direction-specific scan update rates constraints," IET Radar, Sonar & Navigation, vol.12, no.12, pp.1429–1436, 2018.
[5] D.J. Rabideau and P.A. Parker, "Ubiquitous MIMO multifunction digital array radar and the role of time-energy management in radar," MIT Lincoln Lab. Project report DAR-04, 2004.
[6] F.C. Robey, S. Coutts, D. Weikle, J.C. McHarg, and K. Cuomo, "MIMO radar theory and experiment results," IEEE Signals, Systems and Computers, vol.1, pp.300–304, 2004.
[7] V. Mecca, F. Robey, and D. Rabideau, "Phased arrays for multiple-input multiple-output radar," 2016 IEEE International Symposium on Phased Array Systems and Technology, Waltham, MA, 2016.
[8] K. Nishizawa, K. Hirata, S. Kan, H. Miyashita, and S. Makino, "Experimental investigation into grating lobes suppression in distributed array antennas," 2006 International Symposium on Antennas and Propagation, p.201, Nov. 2006.
[9] K. Hirata, K. Nishizawa, S. Matsuda, H. Miyashita, and S. Makino, "Experimental evaluation of Capon's beam former applied to a non-uniformly arranged distributed array," 2006 International Symposium on Antennas and Propagation, pp.202–203, Nov. 2006.
[10] S. Pillai and C.S. Burrus, Array Signal Processing, Spriger-Verlag, 1989.
[11] M.A. Richards, J.A. Scheer, and W.A. Holm, Principles of Modern Radar, SciTech Publishing, 2010.
[12] S.M. Sherman and D.K. Barton, Monopulse Principles and Techniques, 2nd ed., Artech House, 2011.
[13] T. Ito, R. Takahashi, and K. Hirata, "An antenna arrangement for phase comparison monopulse DOA estimation using nonuniform planar array," 2011 European Radar Conference, pp.277–280, 2011.
[14] S.M. Key, Fundamentals of Statistical Signal Processing, Prentice Hall, 1993.
[15] M.A. Richards, Fundamentals of Radar Signal Processing, 2nd ed. McGraw-Hill Education, 2014.
[16] P. Stoica and N. Nehorai, "Music, maximum likelihood and Cramer-Rao bound," IEEE Trans. Acoust., Speech, Signal Process., vol.ASSP-37, no.5, pp.720–741, 1989.
[17] A. Satish, R.L. Kashyap, "Maximum likelihood estimation and Cramer-Rao bounds for direction of arrival parameters of a large sensor array," IEEE Trans. Antennas Propag., vol.44, no.4, pp.478–491, 1996.
[18] R. Takahashi, T. Inaba, T. Takahashi, and H. Tasaki, "Digital monopulse beamforming for achieving the CRLB for angle accuracy," IEEE Trans. Aerosp. Electron. Syst., vol.54, no.1, pp.315–323, 2018.

Appendix A: Identity of ΣΔBF and MLE

In this appendix, the signal model in this study is applied to conventional DOA estimation using MLE [16], [17]. As in the ΣΔBF formulation, the assumptions of a single target, far-field, single snapshot, and non-multipath environment are applied. The log-likelihood $\ln f_{ML}$ can be expressed as

$$\ln f_{ML} = -M \ln\left(\pi\sigma^2\right) - \frac{1}{\sigma^2}\left(\boldsymbol{x}_{\Sigma\Delta} - 4\boldsymbol{a}_{\Sigma\Delta}s\right)^{\mathrm{H}}\left(\boldsymbol{x}_{\Sigma\Delta} - 4\boldsymbol{a}_{\Sigma\Delta}s\right) \quad (\mathrm{A}\cdot 1)$$

the maximum likelihood estimator of s is given by

$$s = \left(4\boldsymbol{a}_{\Sigma\Delta}{}^{\mathrm{H}}\boldsymbol{a}_{\Sigma\Delta}\right)^{-1}\boldsymbol{a}_{\Sigma\Delta}{}^{\mathrm{H}}\boldsymbol{x}. \tag{A·2}$$

Because the MLE is the maximization of the second term on the right-hand side of Eq. (A· 1) by substituting Eq. (A· 2) into it, the MLE becomes the minimization problem of F_{ML} shown as follows:

$$F_{\mathrm{ML}} = \mathrm{tr}\left\{\left(\boldsymbol{I} - \frac{\boldsymbol{a}_{\Sigma\Delta}\boldsymbol{a}_{\Sigma\Delta}{}^{\mathrm{H}}}{\boldsymbol{a}_{\Sigma\Delta}{}^{\mathrm{H}}\boldsymbol{a}_{\Sigma\Delta}}\right)\boldsymbol{x}_{\Sigma\Delta}\boldsymbol{x}_{\Sigma\Delta}{}^{\mathrm{H}}\right\}. \tag{A·3}$$

Equation (A· 3) is rearranged using the property of trace $\mathrm{tr}\left(\boldsymbol{a}\left(\boldsymbol{a}^{\mathrm{H}}\boldsymbol{B}\right)\right) = \boldsymbol{a}^{\mathrm{H}}\boldsymbol{B}\boldsymbol{a}$ as follows:

$$\begin{aligned} F_{ML} &= \mathrm{tr}\left(\boldsymbol{x}_{\Sigma\Delta}\boldsymbol{x}_{\Sigma\Delta}^{\mathrm{H}} - \frac{\boldsymbol{a}_{\Sigma\Delta}\boldsymbol{a}_{\Sigma\Delta}{}^{\mathrm{H}}}{\boldsymbol{a}_{\Sigma\Delta}{}^{\mathrm{H}}\boldsymbol{a}_{\Sigma\Delta}}\boldsymbol{x}_{\Sigma\Delta}\boldsymbol{x}_{\Sigma\Delta}^{\mathrm{H}}\right) \\ &= \mathrm{tr}\left(\boldsymbol{x}_{\Sigma\Delta}\boldsymbol{x}_{\Sigma\Delta}^{\mathrm{H}}\right) \\ &\quad - \frac{1}{\boldsymbol{a}_{\Sigma\Delta}{}^{\mathrm{H}}\boldsymbol{a}_{\Sigma\Delta}} tr\left(\boldsymbol{a}_{\Sigma\Delta}\left(\boldsymbol{a}_{\Sigma\Delta}{}^{\mathrm{H}}\boldsymbol{x}_{\Sigma\Delta}\boldsymbol{x}_{\Sigma\Delta}^{\mathrm{H}}\right)\right) \\ &= \mathrm{tr}\left(\boldsymbol{x}_{\Sigma\Delta}\boldsymbol{x}_{\Sigma\Delta}^{\mathrm{H}}\right) - \frac{\boldsymbol{a}_{\Sigma\Delta}{}^{\mathrm{H}}\boldsymbol{x}_{\Sigma\Delta}\boldsymbol{x}_{\Sigma\Delta}^{\mathrm{H}}\boldsymbol{a}_{\Sigma\Delta}}{\boldsymbol{a}_{\Sigma\Delta}{}^{\mathrm{H}}\boldsymbol{a}_{\Sigma\Delta}}. \end{aligned} \tag{A·4}$$

Because the first term on the right side corresponds to the observed value, the MLE minimizes the second term. Therefore, it can be shown that the MLE estimators $\hat{\theta}_{\mathrm{ML}}$, $\hat{\phi}_{\mathrm{ML}}$ and ΣΔBF with estimators $\hat{\theta}_{\Sigma\Delta}$, $\hat{\phi}_{\Sigma\Delta}$ are consistent as follows:

$$\begin{aligned} \left\{\hat{\theta}_{\mathrm{ML}}, \hat{\phi}_{\mathrm{ML}}\right\} &= \arg\min F_{ML} \\ &= \arg\max \frac{\boldsymbol{a}_{\Sigma\Delta}{}^{\mathrm{H}}\boldsymbol{x}_{\Sigma\Delta}\boldsymbol{x}_{\Sigma\Delta}^{\mathrm{H}}\boldsymbol{a}_{\Sigma\Delta}}{\boldsymbol{a}_{\Sigma\Delta}{}^{\mathrm{H}}\boldsymbol{a}_{\Sigma\Delta}} \\ &= \left\{\hat{\theta}_{\Sigma\Delta}, \hat{\phi}_{\Sigma\Delta}\right\}. \end{aligned} \tag{A·5}$$

Appendix B: CRLB of ΣΔBF and ΣBF

A brief flow of the CRLB calculation used in 4.1 and 4.2 is shown in this appendix. The Fisher information matrix $\boldsymbol{J}$ is defined as follows [14], [18].

$$[\boldsymbol{J}]_{ij} = J_{ij} = E\left[\frac{\partial \ln f_{\mathrm{ML}}(\boldsymbol{q})}{\partial q_i}\frac{\partial \ln f_{\mathrm{ML}}(\boldsymbol{q})}{\partial q_j}\right] \tag{A·6}$$

where $i = 1, \cdots, 5$ and $j = 1, \cdots 5$ are the index numbers, $\ln f_{\mathrm{ML}}(\boldsymbol{q})$ in the case of ΣΔBF represented by Eq. (A· 1), and $\boldsymbol{q}$ is a parameter vector containing five unknown parameters as shown below:

$$\begin{aligned} \boldsymbol{q} &= [q_1, q_2, \cdots, q_5]^{\mathrm{T}} \\ &= \left[u, v, \mathrm{Re}[s], \mathrm{Im}[s], \sigma^2\right]^{\mathrm{T}}. \end{aligned} \tag{A·7}$$

Using $\boldsymbol{J}$ calculated from Eq. (A· 6), the CRLB of the elevation angle accuracy σ_θ is given by

$$\boldsymbol{C}_{\theta,\phi} = \frac{\partial\boldsymbol{\theta}}{\partial\boldsymbol{q}}\boldsymbol{J}^{-1}\left(\frac{\partial\boldsymbol{\theta}}{\partial\boldsymbol{q}}\right)^{\mathrm{T}} \tag{A·8}$$

$$\sigma_\theta = \sqrt{\left|\boldsymbol{C}_{\theta,\phi}\right|_{11}} \tag{A·9}$$

where $\boldsymbol{\theta} = \left[\theta \quad \phi\right]^{\mathrm{T}}$. It should be noted that θ and ϕ represented by the elements of $\boldsymbol{q}$ can be written as

$$\theta = \sin^{-1} v \tag{A·10}$$

$$\phi = \sin^{-1}\frac{u}{\sqrt{1-v^2}}. \tag{A·11}$$

In the case of ΣBF, substituting $\boldsymbol{x}_{\Sigma\Delta} = \boldsymbol{x}_{\Sigma}$ and $\boldsymbol{a}_{\Sigma\Delta} = \boldsymbol{a}_{\Sigma}$, calculating Eq. (A· 1), Eq. (A· 5), Eq. (A· 8), and Eq. (A· 9), the CRLB of ΣBF can be obtained using the same procedure as ΣΔBF.

Appendix C: GL Suppression Effect by Random Arrangement and Evaluation Results

In 4., performance evaluation is conducted using the SA arrangement shown in Fig. 6. In the arrangement, a random arrangement is applied within each of the upper and lower regions, and the apertures in each region have a slight aperture length in the height direction. The DBF beam pattern of the entire SA arrangement asymptotically approaches the product of the pattern of two antennas separated by ΔH in the height and the pattern of apertures in each of these regions. In other words, the apertures in each region provide slight GL suppression. The two antennas with ΔH separation alone generate GL without loss as in Fig. 2. However, the multiplication of the pattern of apertures in each region causes a slight level reduction in GL.

To confirm this effect, Fig. A· 1 and Fig. A· 2 show the results of evaluating the DBF beam pattern for the SA arrangement in Fig. 6. The horizontal axis is the elevation angle, whereas the vertical axis is the power normalized at the DBF beam direction. Figure A· 1 shows the result of $\Delta H = 25\lambda$ and Fig. A· 2 shows the result of $\Delta H = 40\lambda$. Both results show lower GL levels than the subarray pattern. The GL suppression effect described above can be confirmed.

Additionally, Fig. A· 1 has a greater reduction effect than Fig. A· 2. According to Eq. (1), θ_{GL} increases as ΔH decreases. However, the level of the pattern of the apertures

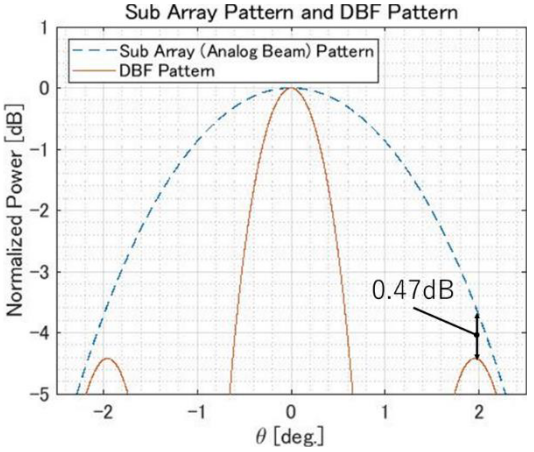

Fig. A· 1 Sub array pattern and DBF pattern of the SA arrangement shown in Fig. 6 in case ΔH is 25λ.

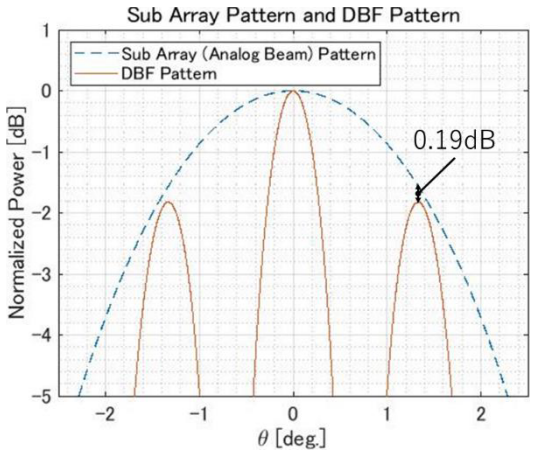

Fig. A· 2 Sub array pattern and DBF pattern of the SA arrangement shown in Fig. 6 in case ΔH is 40λ.

in each region decreases as the angle increases. Therefore, the GL suppression effect increases as ΔH decreases.

Toshihiro Ito received the B.E. and M.E. degrees in Electrical Engineering from Kanazawa University in 2006 and 2008. He is now with the Information Technology R&D Center, Mitsubishi Electric Corp., and the Graduate School of Natural Science and Technology, Kanazawa University. His research interests are radar signal processing, adaptive array signal processing, and DBF array radar systems. He is a member of the Institute of Electronics, Information and Communication Engineers (IEICE).

Shoji Matsuda received the B.E., M.E. and Ph.D. degrees in the field of electrical engineering from Kyoto University in 1976, 1978, and 2006 respectively. He is now with the Communication Systems Center, Mitsubishi Electric Corp, and e participating in the development of a large radar system. He is a member of the Institute of Electronics, Information and Communication Engineers (IEICE), and the Institute of Electrical and Electronic Engineers (IEEE).

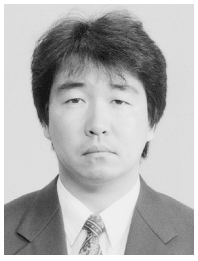

Yoshiya Kasahara received the B.E., M.E. and Ph.D. degrees in the field of electrical engineering from Kyoto University in 1989, 1991, and 1996, respectively. He is currently a professor and director in the Emerging Media Initiative, Kanazawa University. His research interests are radio engineering and radio science, intelligent signal processing for the measurements of plasma waves onboard spacecraft, theoretical studies on generation and propagation mechanism of waves in space plasma, and database systems for the space environment. He is a member of the Institute of Electronics, Information and Communication Engineers (IEICE), Society of Geomagnetism and Earth, Planetary and Space Sciences (SGEPSS), Information Processing Society of Japan (IPSJ) and American Geophysical Union (AGU).